USM3D-ME Buffet Simulations of the ONERA OAT15A Airfoil for DPW-8/AePW-4

Tausif Jamal*, Brent Pomeroy†, and Seth Kelly‡
NASA Langley Research Center, Hampton, VA, 23681, USA

Numerical simulations of transonic flow over the ONERA OAT15A airfoil using the USM3D-ME solver are carried out in support of the DPW-8/AePW-4 Buffet Working Group Test Case 1a. The aim of this paper is to investigate Reynolds-averaged Navier-Stokes (RANS) model performance for transonic buffet. Two different families of committee-supplied grids developed by Cadence and Helden Aerospace are investigated at a Mach Number (M_∞) of 0.73 and a chord Reynolds Number of 3.0×10^6. Results indicate that the two families of grids provide different solutions based on their respective mesh generation philosophy. Although grid convergence is achieved for Cadence grids, no oscillatory behavior associated with buffet is observed. In comparison, grid convergence is not achieved for the HeldenMesh grids due to the presence of oscillations in the flow field. The HeldenMesh grid solutions also predict the shock content in an improved manner due to the increased mesh density around the shock location. Based on the results, it is demonstrated that RANS models are able to capture the pre-buffet conditions and the onset of buffet with some accuracy, however temporal accuracy is a necessity for the prediction of accurate physics associated with buffet.

I. Nomenclature

AePW = Aeroelastic Prediction Workshop
AIAA = American Institute of Aeronautics and Astronautics
α = Angle of Attack, degrees
BC = Boundary Condition
c = Chord length
C_d = Drag Coefficient
C_l = Lift Coefficient
C_p = Pressure Coefficient
CFD = Computational Fluid Dynamics
DES = Detached Eddy Simulation
DNS = Direct Numerical Simulation
DPW = Drag Prediction Workshop
FDS = Flux-Difference-Splitting
HANIM = Hierarchical Adaptive Non-Linear Iteration Method
HRL = Hybrid RANS-LES
LES = Large-Eddy Simulation
M_∞ = Freestream Mach number
NASA = National Aeronautics and Space Administration
ONERA = Office National d'Études et de Recherches Aérospatiales
PA = Preconditioner Alone Solver
Re_c = Mean Chord Reynolds Number
RANS = Reynolds-averaged Navier-Stokes
SA = Spalart-Allmaras baseline turbulence model
SA-Neg = Negative version of Spalart-Allmaras turbulence model
QCR = Quadratic Constitutive Relation
SA-Neg-R = Spalart-Allmaras Negative turbulence model with Rotation Correction

SST k-ω = Shear-Stress Transport *k-ω* turbulence model
TTBW = Transonic Truss-Braced Wing
URANS = Unsteady Reynolds-averaged Navier-Stokes
WMLES = Wall-Modeled Large-Eddy Simulation

* Configuration Aerodynamics Branch, tausif.jamal@nasa.gov.
† Configuration Aerodynamics Branch, AIAA Senior Member, brent.w.pomeroy@nasa.gov.
‡ Configuration Aerodynamics Branch, AIAA Member, seth.w.kelly@nasa.gov.

II. Introduction

Understanding the aerodynamics associated within the flight envelopes of commercial aircraft is of paramount importance for research and development. Since most commercial aircrafts operate at transonic speeds, it is therefore important to understand the complex flow physics associated with this flow regime which is characterized by the presence of both, subsonic and supersonic flow. One of the main physical phenomena that limits the performance of transonic flight is buffet. As the supersonic flow over an aircraft decelerates to subsonic speeds, a discontinuity is formed known as a shockwave. Aft of the shockwave, a region of boundary layer separation is often observed which is marked by the shock foot terminating on the surface of the lifting body. Transonic buffet occurs when the shock enters a self-sustaining motion on the surface of an airfoil as a result of its interaction with the boundary layer. This instability may induce structural vibrations which are detrimental to the aerodynamic performance of the lifting body and may lead to structural damage if not mitigated.

Over the last few decades, various attempts at characterizing and predicting buffet have been carried out by experimental and numerical methods. The multidisciplinary American Institute of Aeronautics and Astronautics (AIAA) Drag Prediction Workshop 8 and Aeroelastic Prediction Workshop 4 (DPW-8/AePW-4) is composed of seven different working groups, one of which is the Buffet Working Group [1]. The Buffet Working Group includes experts from both the DPW and AePW communities. The goal of this working group is to investigate both the pre- and post-buffet environment. This paper focuses on the first test case, Test Case 1a, which includes investigation of transonic buffet of the ONERA OAT15A transonic airfoil, designed by Office National d'etudes et de Recherches Aerospatiales (ONERA) using Reynolds-averaged Navier-Stokes (RANS) models for a large range of angles of attack (α).

Brunet [2,3] performed a comprehensive steady and unsteady numerical investigation of transonic buffet for the ONERA OAT15A airfoil at $M_\infty = 0.73$ using the Spalart-Allmaras (SA) [5], SST *k-ω* [6], and algebraic Reynolds stress models [7]. Results indicated that the Reynolds-stress model provided the best agreement with experimental data, while the SST and the SA models underpredicted and overpredicted the size of the separated zone, respectively. The study also indicated that the SA model also tended to damp out the oscillatory behavior of the flow resulting in delayed prediction of buffet onset. The author concluded that although the RANS models were able to predict the mean-flow features with relative accuracy, agreement with experimental studies was only obtained when the angle of attack was increased in comparison to the experimental value.

Further investigations on the ONERA OAT15A were carried out by Deck [8] who utilized hybrid RANS-LES models with considerable success. The zonal hybrid RANS-LES (HRL) model used in the study was able to predict the periodic motion of the shock and reproduced the buffet phenomena at experimental angle of attack values. Interestingly, the standard Detached-Eddy Simulation (DES) model failed to predict the self-sustaining buffet motion even at higher angles of attack. URANS models were able to predict the buffet motion but, similar to Brunet, they required an increase in angle of attack. Some discrepancies between the zonal DES model predictions and experimental data were observed such as overprediction of the wall pressure and the prediction of an advanced shock location compared to experiment. Overall, it was concluded that the zonal DES approach was significantly more successful in predicting this complex physical phenomenon than traditional URANS and DES methods. It must be noted that the failure of DES in that study is likely a direct result of DES being developed to handle strong separated regions accompanied by large scales of motion. Transonic buffet is associated with thin-layer instabilities which have traditionally proven to be challenging for the hybrid RANS-LES approach. This drawback of hybrid RANS models can be due to a number of different reasons such as the inaccurate shielding of RANS, lack of resolved turbulence, and weak RANS-LES coupling. An alternative to the zonal DES method would be to employ the dynamic Hybrid RANS-LES model [9-10] with exponential filtering [11-12], to accurately resolve the oscillatory nature of the flow field.

Recently, several studies conducted by NASA Ames Research Center have provided valuable insight into the performance of URANS, HRL, and Wall-Modeled LES (WMLES) for predicting transonic buffet. Haas et al. [13] questioned the efficacy of using WMLES for buffet prediction when URANS was able to closely match experimental

observations for only a fraction of the cost. Additionally, the complications involving appropriate grid generation techniques and the choice of correct numerics to predict these types of flows with WMLES makes URANS a more attractive alternative.

Browne et al. [14] conducted investigations to evaluate the performance of HRL models in predicting buffet for the SUGAR Transonic Truss Braced Wing (TTBW). The HRL model predictions agreed with experimental observations closely when predicting integrated loads in the post-pitch-break region when compared to URANS which tended to underpredict lift. Although both URANS and HRL models predicted shock formation downstream of experimental observations in the pre-pitch-break region, the HRL model was able to predict the shock location with more accuracy in the post-pitch-break region. One major drawback of the HRL models was the prediction of excessively large flow separation zones. It was concluded that further studies with finer grids were required to properly assess the performance of HRL models for these types of flow.

Maldonado et al. [15] proposed a physics-based approach to numerically determine the onset of transonic buffet. The study predicts buffet onset by analyzing time-series data of integrated loads based on a moving-body, continuously pitched approach. Simulations using URANS coupled with various low-dissipation convective flux formulations [16-19] were carried out for NACA0012 and ONERA OAT15A airfoils. Results indicated that the onset of buffet was significantly affected by the type of convective flux discretization utilized. The authors suggested using a low-dissipation convective flux formulation since buffet requires a numerical scheme to resolve these natural instabilities. Additionally, time-step sensitivity analysis indicated that the large time-steps may often delay the onset of buffet. Finally, sensitivity of buffet onset angle to problem-setup revealed that a decrease in pitch rate of the moving body analysis resulted in earlier buffet onset and improved predictive capabilities when compared to theoretical and prior numerical results, however a slower pitch-rate also required increased computational overhead.

These past studies indicate that successful prediction of transonic buffet requires an appropriate blend of turbulence models, numerics, solver, and solution setup. Although scale-resolving simulations are able to resolve more physics, URANS based methods are still able to predict the onset of transonic buffet in addition to providing a relatively good approximation of integrated loads. However, this study is restricted to only steady-state computations i.e., RANS simulations to build a platform for further investigations using URANS and HRL methods in the future. In this study, the predictive capabilities of three variants of the SA [5] turbulence model are compared against experimental studies. Parametric studies are performed using two families of mixed-element (ME) grids generated using HeldenMesh [20] and Cadence [21] and supplied by AIAA Drag Prediction Workshop-8 (DPW-8) organizing committee. Results from the numerical studies are compared against each of the grid families and experimental data [22].

III. Problem Description

The current study includes Test Case 1a for the supplemental Buffet Working Group for the AIAA DPW-8/AePW-4. The test case involves transonic flow over the ONERA OAT15A airfoil which has provided a platform for the research community to investigate transonic buffet over the past two decades. Experimental studies were carried out by Jacquin et al. [22] in 2009 to study shock oscillation in ONERA's Meudon Center's continuous closed-circuit transonic S3Ch wind tunnel. The test section dimensions were 0.78 m x 0.78 m x 2.2 m (length, height, width) and the OAT15A airfoil (see Fig.1) has a chord length of 0.23 m with a maximum thickness-to-chord ratio of 12.3% and trailing edge thickness of 0.50%.

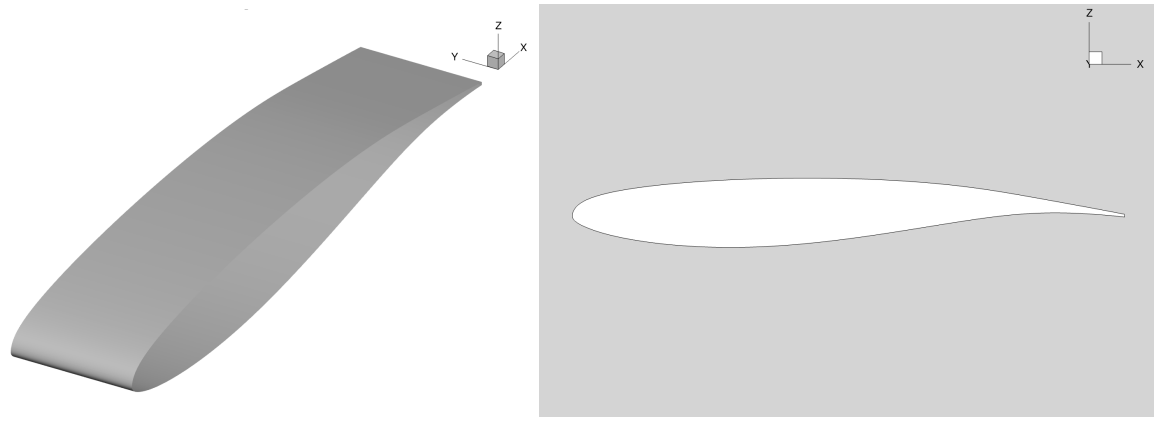

Figure 1. The ONERA OAT15A airfoil.

The simulation conditions were identical to the experiment which was carried out at M_∞=0.73 for a mean-chord Reynolds number (Re_c) of $3x10^6$. Additionally, an angle of attack range of 1.36º - 3.90º was provided to determine pre- and post-buffet characteristics since the experimentally determined buffet onset was at α ~3.00º. Table 1 provides a detailed list of all simulation parameters.

Table 1. Simulation Parameters.

Angle of Attack	Reynolds number (Re_c)	Freestream Static Temperature	Mach Number
1.36º, 1.50º, 2.50º, 3.00º, 3.10º, 3.25º, 3.40º, 3.50º, 3.60º, and 3.90º	$3.0x10^6$	487.8 ºR	0.73

Grids were provided by the organizing committee to preserve uniform standards for all the participants; however, each participant was given the option to generate their own grids. The two families of grids used in this study were generated by Cadence and HeldenMesh. Each grid family contained six entries, namely: tiny (L1), coarse (L2), medium (L3), fine (L4), extra-fine (L5), and ultra-fine (L6). Figure 2 shows the computational domain for the Cadence and HeldenMesh families of grids, respectively. The dimensions provided are in terms of chord length (c).

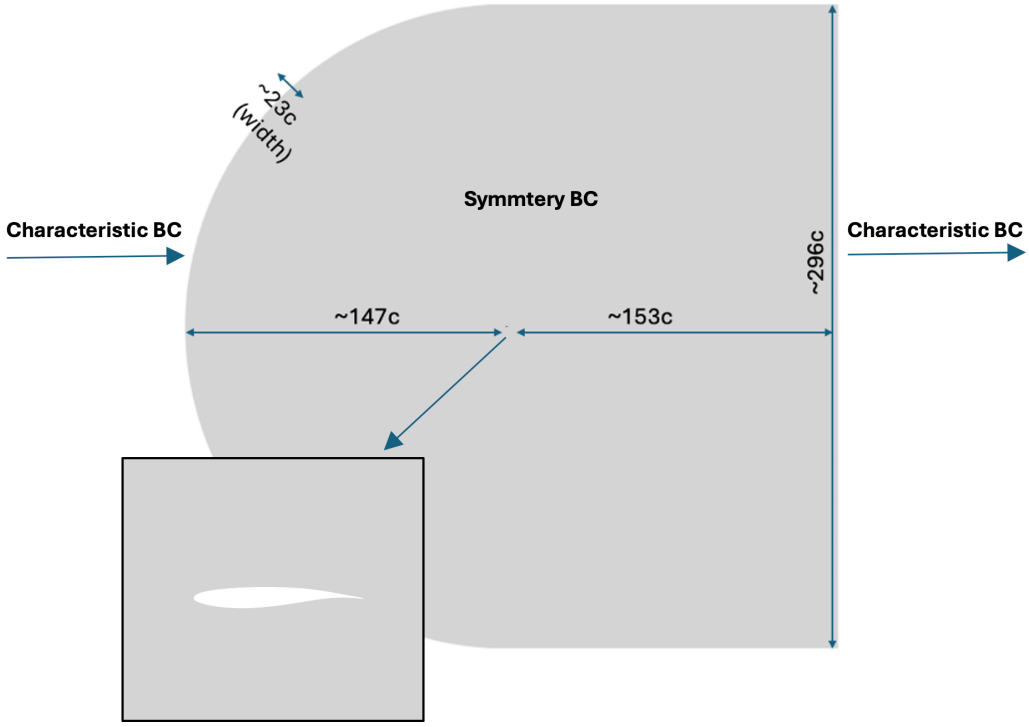

(a) Computational domain for the Cadence family of grids

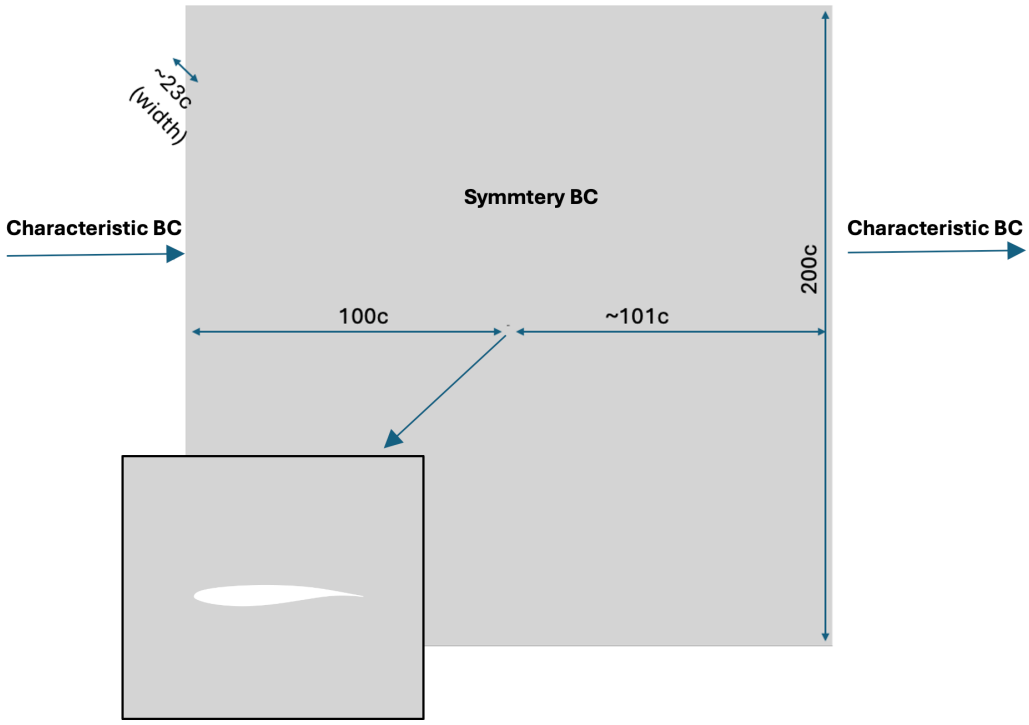

(b) Computational domain for the HeldenMesh family of grids

Figure 2. Comparison of the computational domains used in this study.

Both Cadence and HeldenMesh families are mixed element grids containing prisms outside the boundary layer and quadrilateral cells inside the boundary layer. Both grids are 1-cell wide with all triangular faces of the prisms projected on the symmetry planes (spanwise direction). Tables 2 and 3, shown below, highlight the cell density in each of the grids generated by the two grid partners.

Table 2. Cell Density for Cadence Grids.

Grid	Cadence (Cells)	y^+
L1	0.47×10^5	1.000
L2	0.89×10^5	0.670
L3	1.50×10^5	0.500
L4	2.35×10^5	0.400
L5	3.53×10^5	0.330
L6	5.17×10^5	0.290

Table 3. Cell Density for HeldenMesh Grids.

Grid	HeldenMesh (cells)	y^+
L1	0.10×10^5	4.000
L2	0.35×10^5	2.000
L3	1.34×10^5	1.000
L4	5.28×10^5	0.500
L5	20.76×10^5	0.250
L6	82.08×10^5	0.125

From Tables 2 and 3, it is evident that there are some differences in the total cell count for each of the grid families. To avoid any major differences in results arising from differences in cell distribution between the two grid families and to reduce computational overhead, this study only compares performance of grid levels L1, L2, and L3.

Figure 3 compares the mesh distribution around the ONERA OAT15A airfoil for the Cadence and HeldenMesh family of grids. While the committee provided gridding guidelines, these were not requirements. Consequently, the grid partners explored different meshing techniques with the approaches taken by the two grid partners varying significantly. The Cadence grids use lower growth rates and the stretching inside the boundary layers is relatively uniform all around the airfoil with a shock refinement zone on the suction side. The HeldenMesh grids in comparison, contain tightly packed cells in the streamwise direction on the suction side with a shock-cone type refinement zone. The HeldenMesh grids also have significantly larger growth ratios away from the airfoil making the far-field regions significantly coarser than the Cadence grids.

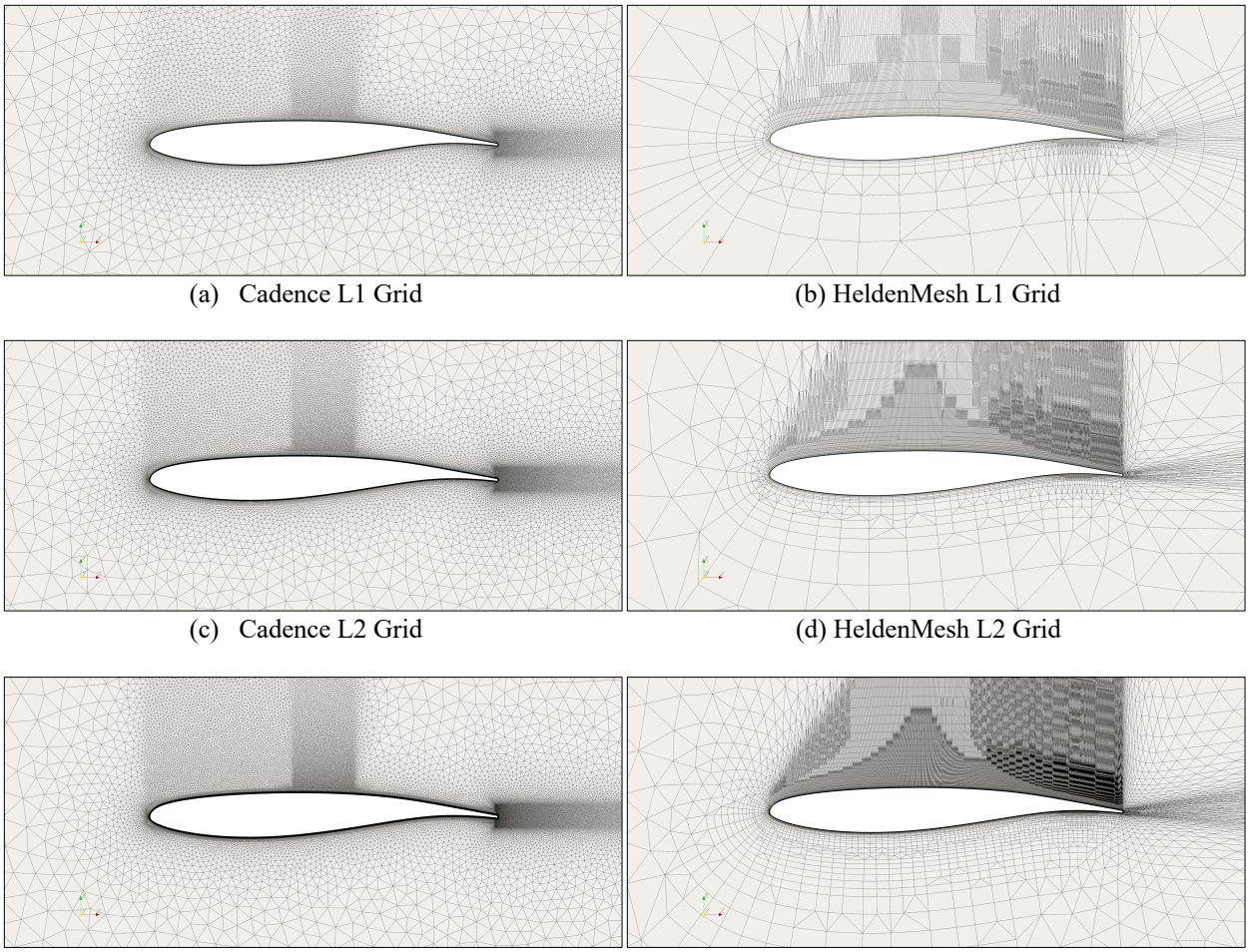

(a) Cadence L1 Grid (b) HeldenMesh L1 Grid

(c) Cadence L2 Grid (d) HeldenMesh L2 Grid

(e) Cadence L3 Grid (f) HeldenMesh L3 Grid

Figure 3. Comparison of the Cadence and HeldenMesh family of grids in the vicinity of the airfoil.

IV. Turbulence Modeling

Aerodynamics often includes complex features such as turbulent wakes, vortices, adverse pressure gradients, and regions of varying turbulence intensities. The presence of these types of complex flow phenomena makes prediction of aerodynamic flows a daunting task for turbulence models. The modern turbulence modeling approaches can be broadly classified into three overarching approaches: RANS, LES, and Direct Numerical Simulation (DNS). The RANS approach revolves around solving the ensemble-averaged Navier-Stokes equations. This results in unclosed terms which are then modeled to obtain a solution. RANS does not explicitly resolve any scales of motion, instead all scales are modeled to obtain their average contribution to turbulent stresses. LES explicitly resolves some scales of

motion, while Direct Numerical Simulation (DNS) explicitly resolves all scales of motion. The cost and accuracy associated with these methods are directly proportional to the range of scales resolved with RANS being the cheapest and DNS being the most expensive. For most engineering problems, RANS is the preferred method due to computational efficiency and ease of setup. However, recently there has been an increase in the use of HRL and WMLES for certain aerospace problems where RANS models have been found to underperform. One such example is the complex flow associated with high-lift configurations where slat, wing, flap, and bracket interaction results in the presence of unsteady boundary layers with regions of highly separated flow [23].

For the current investigation, variants of the Spalart-Allmaras (SA) RANS turbulence model have been used. The SA [4], one-equation turbulence model has been extensively validated and verified for numerous aerospace applications since its inception in 1992. The SA model solves a transport equation for modified vorticity ($\tilde{\nu}$) which is used to close the RANS equations. The SA-Neg [24] variant used in this study was developed to address some of the shortcoming of the baseline SA model which tended to produce non-physical turbulent viscosity in under-resolved grids, in boundary layer transition regions, and in wakes. The SA-Neg model solves a modified equation that includes provisions for when the baseline model predicts negative turbulent viscosity. In this case, the model treats $\tilde{\nu}$ as a passive scalar eliminating the issues associated with the baseline SA model. Additionally, performance of the SA-Neg model with Rotation (SA-Neg-R) correction is also evaluated. The rotation correction was proposed by Dacles-Mariani et al. [25-26] to account for system rotation and streamline curvature. The model includes a modification for the production term that reduces turbulence production when vorticity exceeds strain-rate. Finally, the performance of the Quadratic Constitutive Relation (QCR) version of the SA model is also investigated. The QCR correction was developed by Spalart [27] in 2000 to address shortcomings of the linear eddy viscosity turbulence model in predicting flows with stress anisotropy. The current study utilizes the baseline QCR formulation dubbed the SA-Neg-QCR-2000. Note that SA-Neg-QCR2000 model is referred to as the SA-Neg-QCR model in this paper.

V. Solver

Steady-state RANS simulations were carried out using the finite volume solver USM3D-ME [28-32]. USM3D-ME is the mixed element version of the legacy USM3D solver developed at NASA Langley Research Center. USM3D-ME utilizes the Hierarchical Adaptive Non-Linear Iteration Method (HANIM) which is a strong solver that significantly increases computational robustness and efficiency [30]. From numerous studies, HANIM has been shown to significantly reduce time/iterations to convergences and provide a deeper convergence when compared to the Preconditioner Alone (PA) solver. The current simulations were run with second order spatial accuracy with the inviscid fluxed discretized using Roe's flux-difference-splitting (FDS) scheme. Additionally, for the HeldenMesh grids, a min-mod limiter has been utilized to provide initial solution robustness for the first 3000 iterations. Cadence grids did not require the use of a limiter and deep convergence was obtained for a majority of the cases.

VI. Results and Discussion

Results for the numerical simulations of the ONERA OAT15A airfoil are discussed in this section including iterative and grid convergence, coefficient of pressure (C_p) comparisons, and shock prediction for each grid family.

A. Solution Convergence

Figures 4-6 highlight the iterative convergence of Cadence L3 grids using the SA-Neg, SA-Neg-R, and the SA-Neg-QCR turbulence model. All the SA-Neg model variants achieve iterative convergence with all the residuals approaching machine zero around 20000 iterations. From numerical and experimental studies, the onset of buffet has been observed to occur at α~3.00º. However, no such behavior is observed for the Cadence family of grids. Figure 7 highlights the grid convergence for the three Cadence grids. Coefficient of drag (C_d) and lift (C_l) converge for the final grid with very miniscule difference in results between L2 and L3.

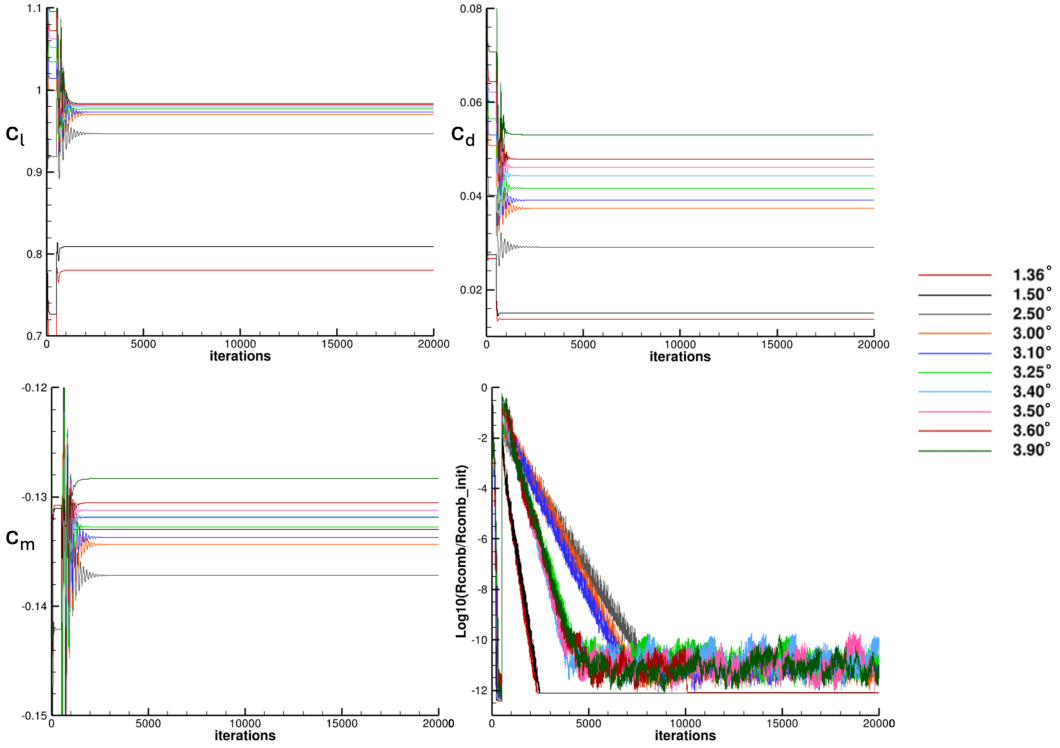

Figure 4. Iterative convergence of C_l, C_d, C_m, and RMS of Residuals for SA-Neg Model on Cadence L3.

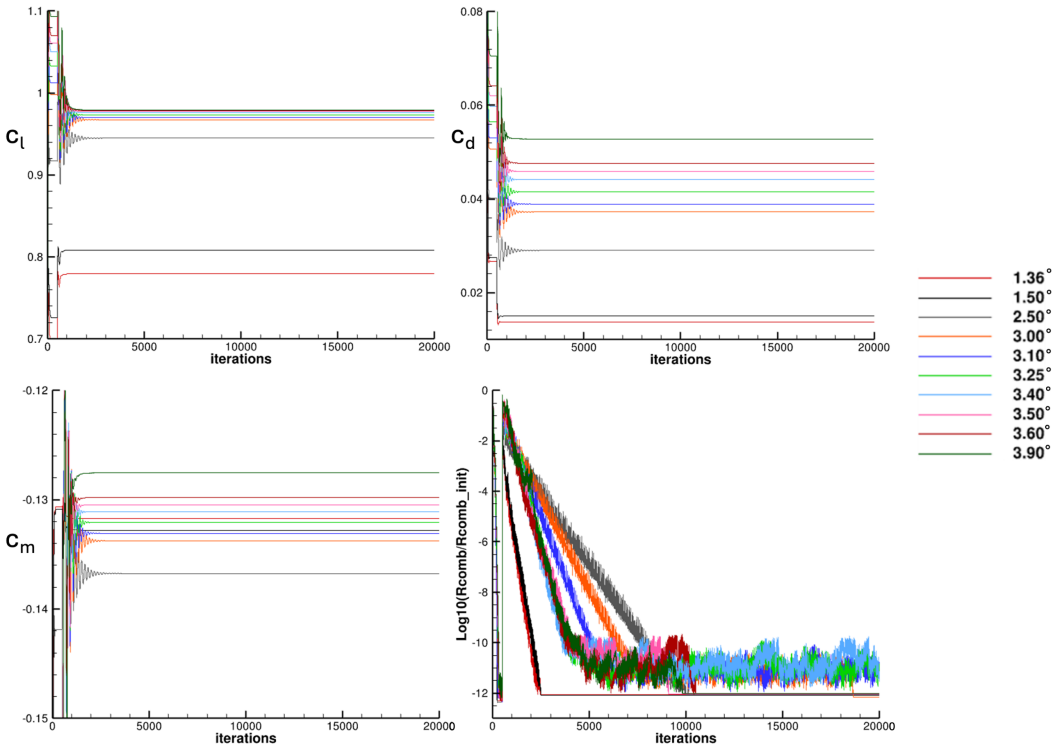

Figure 5. Iterative convergence of C_l, C_d, C_m, and RMS of Residuals for SA-Neg-R Model on Cadence L3.

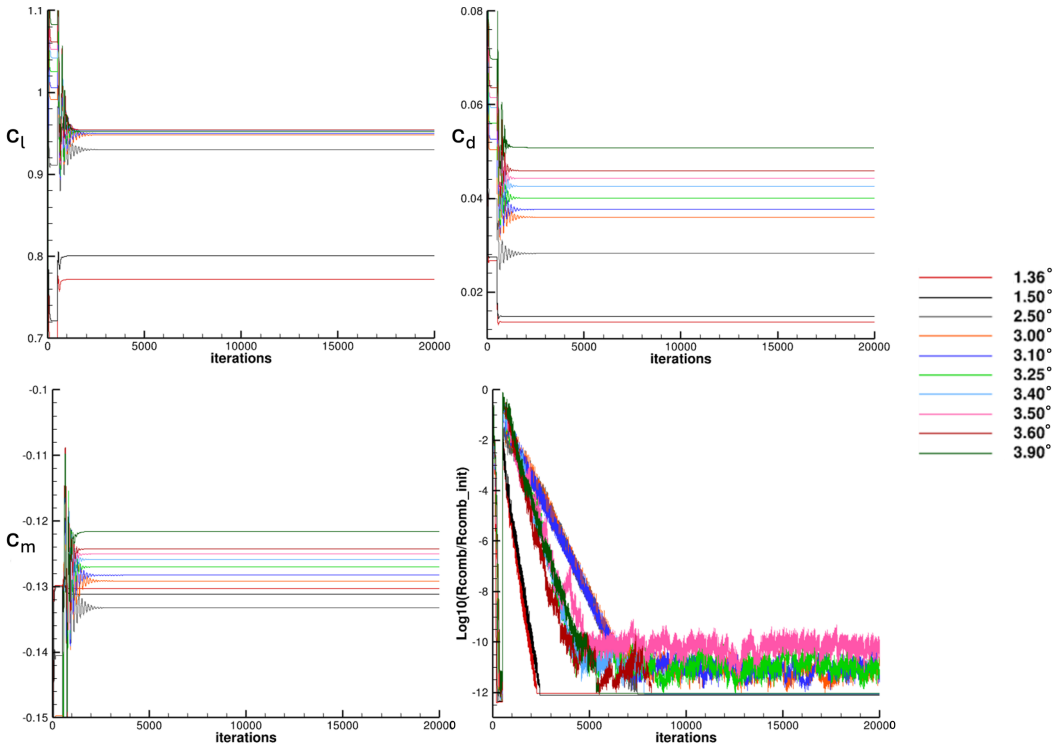

Figure 6. Iterative convergence of C_l, C_d, C_m, and RMS of Residuals for SA-Neg-QCR Model on Cadence L3.

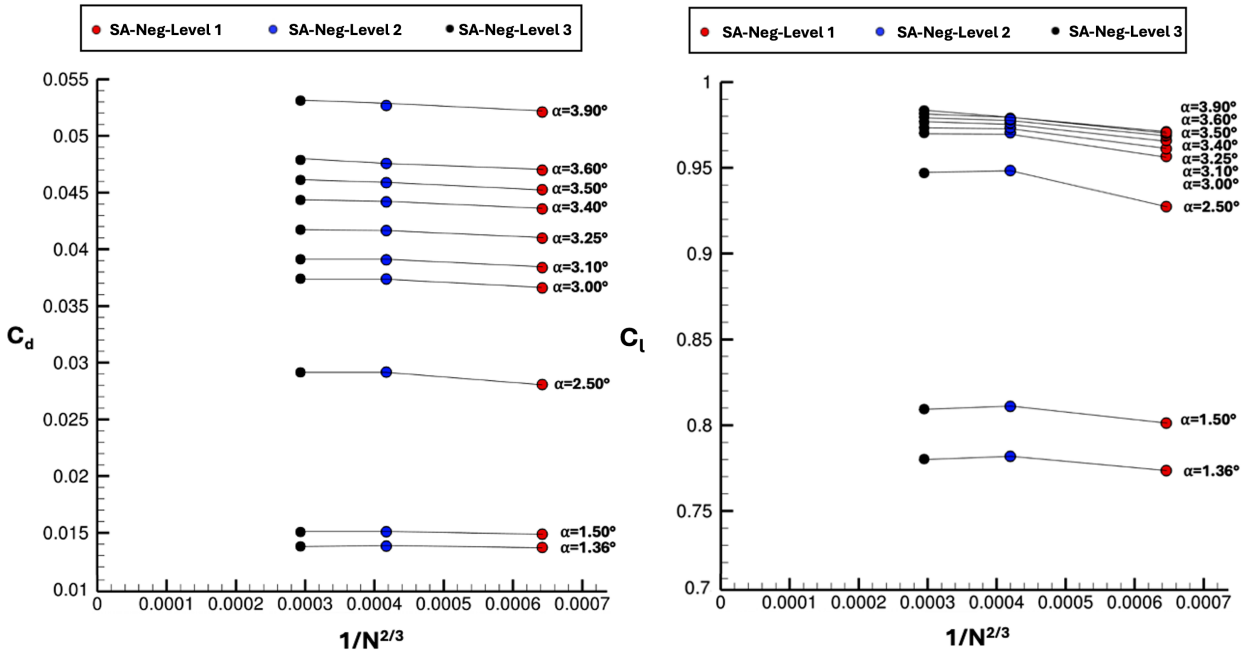

(a) C_d sensitivity to grid resolution (b) C_l sensitivity to grid resolution

Figure 7. Grid convergence of integrated forces for all the Cadence Grids.

Interestingly, iterative convergence for the HeldenMesh grids L1 and L2 was achieved for all angles of attack however, for L3, iterative convergence was obtained only for α =1.36º and 1.50º. Starting at α= 2.50º, oscillations in

integrated forces and pitching moments are observed as shown in Fig.8 below. These oscillations increase in amplitude and wavelength with an increase in α. The oscillatory behavior for α > 1.50º indicates that the HeldenMesh grid L3 predicts an unconverged flow field. This is similar to the observations made by Brunet [2]. It is likely that the instabilities resolved using the HeldenMesh grids are due to the extra refinement on the suction side of the airfoil. Both families of grids were created for RANS type solution however, it is apparent that the HeldenMesh grids are more tailored for an unsteady solution. Figure 9 highlights the iterative convergence behavior for α=2.50º. Since oscillations were observed in the solution, for improved convergence, steady-state solutions were first initialized and run with 1st order spatial accuracy for 40000 iterations then switched to 2nd order.

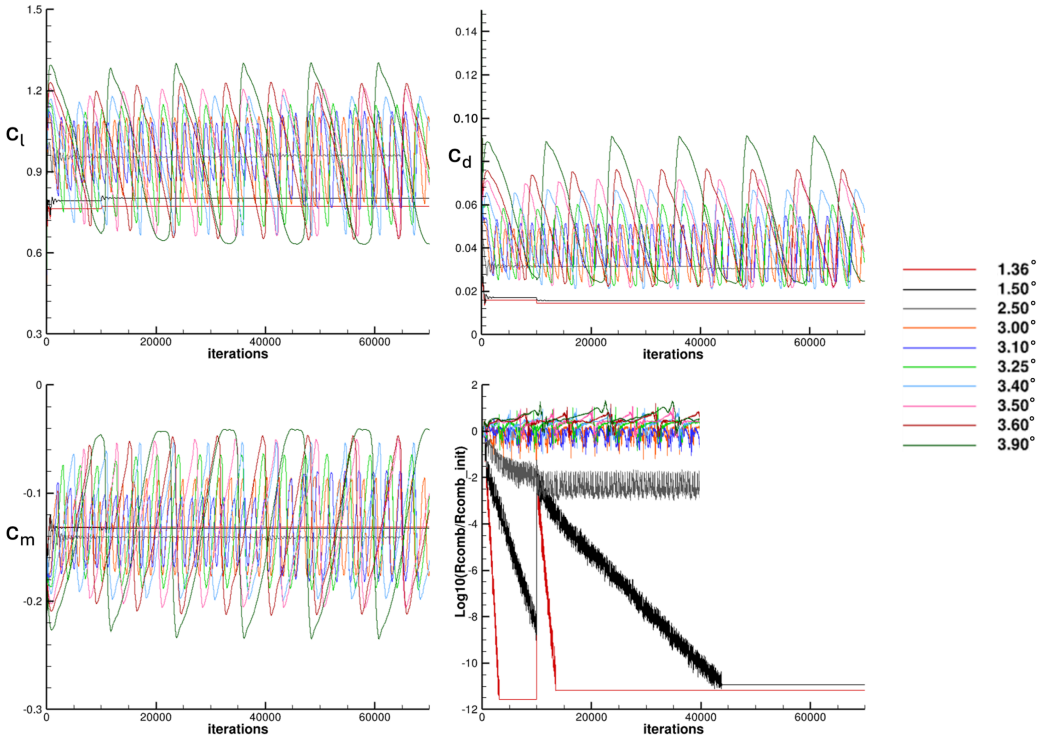

Figure 8. Iterative convergence of C_l, C_d, C_m, and RMS of Residuals for SA-Neg Model on HeldenMeshL3.

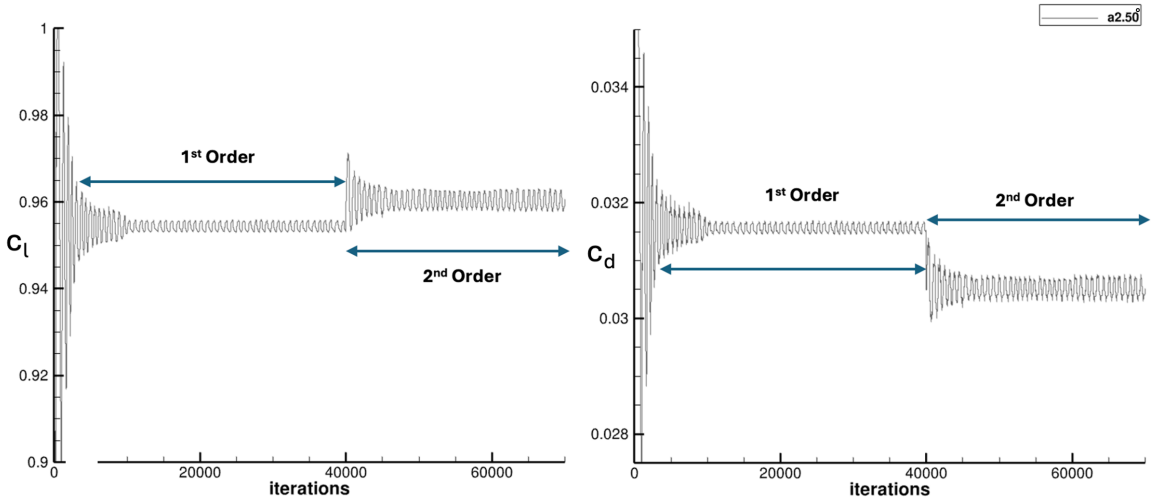

Figure 9. Iterative convergence of C_l, C_d, C_m, and RMS of Residuals for SA-Neg Model for α =2.50º showing the onset of flow instabilities.

Figure 10 shows the grid convergence for the HeldenMesh family of grids. Unlike the Cadence grids, the HeldenMesh grid L3 does not converge. Statistics show some difference between grid L1 to L2 however, major differences are observed going from L2 to L3. To be able to obtain some relevant information from the integrated forces due to their oscillatory nature, results from grid L3 were averaged over the last 10000 iterations.

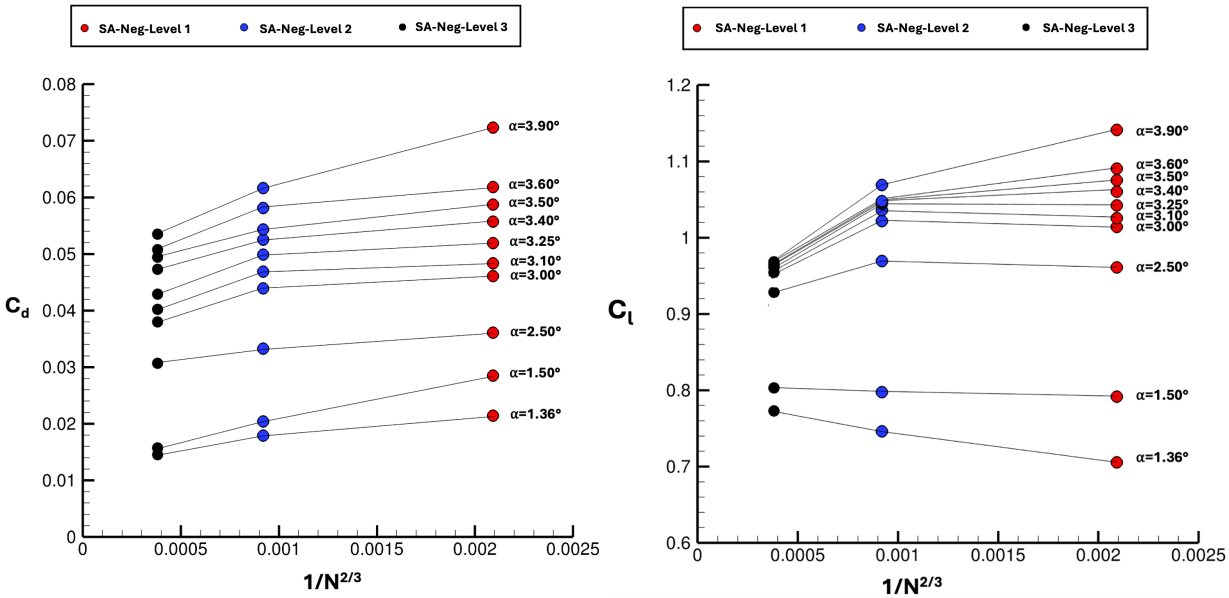

(a) C_d sensitivity to grid resolution (b) C_l sensitivity to grid resolution

Figure 10. Grid convergence of integrated forces for all the HeldenMesh Grids.

C. Pressure Coefficient (C_p) Comparisons

The C_p distribution for the ONERA OAT15A is characterized by the presence of a pressure plateau upstream of the shock. The location of the shock occurs around x/c=0.48 for experiment for α =2.50º to 3.00º. For higher angles of attack the shock starts oscillating and it has been observed to move as far upstream as x/c=0.30 for α =3.90º. A decrease in trailing-edge pressure is also observed as the flow separates during buffet. Additionally, Jacquin et al. [22] stated that the spreading of the compression region results from time-integration of flow intermittency during shock oscillation. Figures 11-14 compare the Cp predictions for the Cadence and HeldenMesh grids.

Figures 11 and 12 compare the predicted Cp profiles by the SA-Neg, SA-Neg-R and SA-Neg-QCR turbulence models for the Cadence grid and predictions from the SA-Neg model for HeldenMesh grids L1 and L2. As observed during the convergence comparisons, the Cadence grids remain relatively insensitive to changes in grid resolution and little-to-no change in C_p is observed, while HeldenMesh results show significant grid sensitivity. One of the major reasons for the difference in C_p from L1 to L2 can simply be attributed to the fact that HeldenMesh L1 grid contains just ~10,000 cells. In reality, it is too coarse to be able to accurately resolve the shock. Despite this, L1 captures the results for α <3.50º relatively well with disagreements only occurring in the vicinity of the shock. Results significantly improve with refinement as L2 results are closer to Cadence results. Interestingly, both families of grids tend to predict the shock location downstream from experimental observations which also results in delayed boundary layer separation. This is also in agreement with Brunet's [2] numerical analysis which showed that SA model predicted the shock location farther downstream than the SST k-ω and Algebraic-Stress Models. Overall, SA-Neg-QCR shows closest agreement with experimental data.

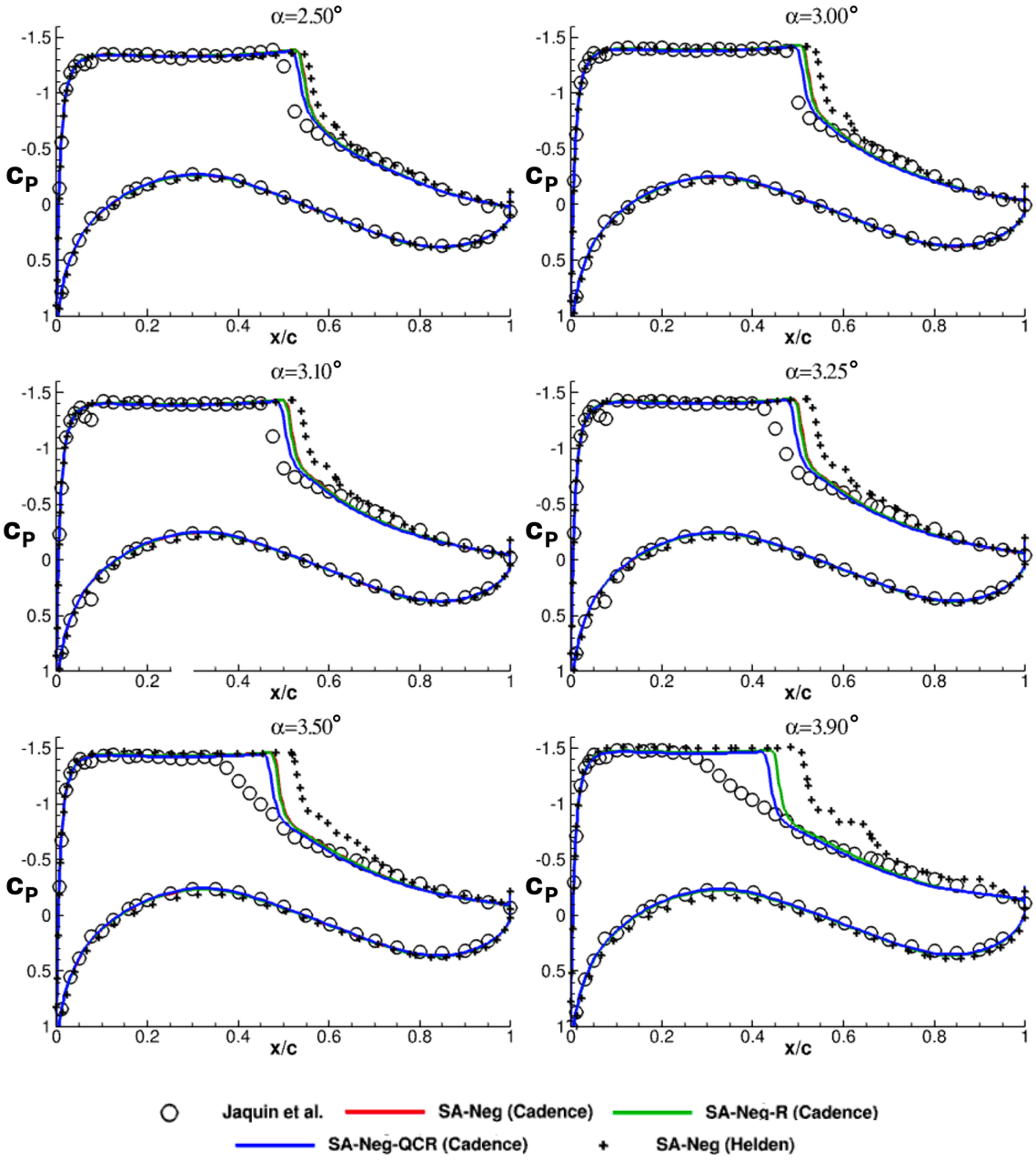

Figure 11. Cp prediction comparison between Cadence L1 and HeldenMesh L1 grids.

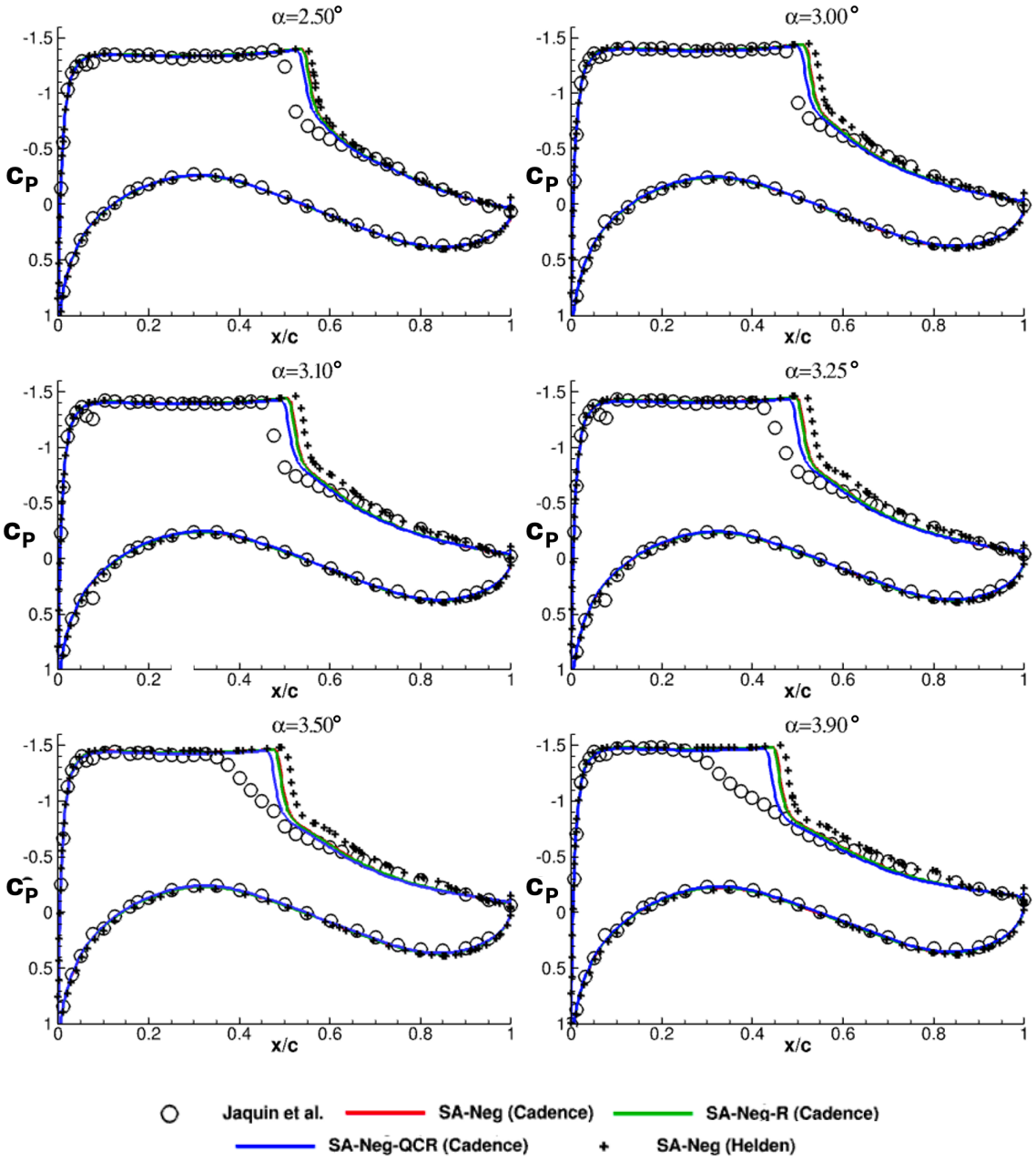

Figure 12. Cp prediction comparison between Cadence L2 and HeldenMesh L2 grids.

From the iterative convergence results, it is evident that HeldenMesh solutions for grid L3 predict unsteadiness. Ideally, a URANS solution with time-averaged quantities would be required for more appropriate comparison with experiments. However, since this study only focuses on steady-state computations, results from HeldenMesh L3 were averaged over one oscillation in their forces once limit-cycle behavior was reached. Figure 13 highlights the C_l and the corresponding Cp behavior for an example flow.

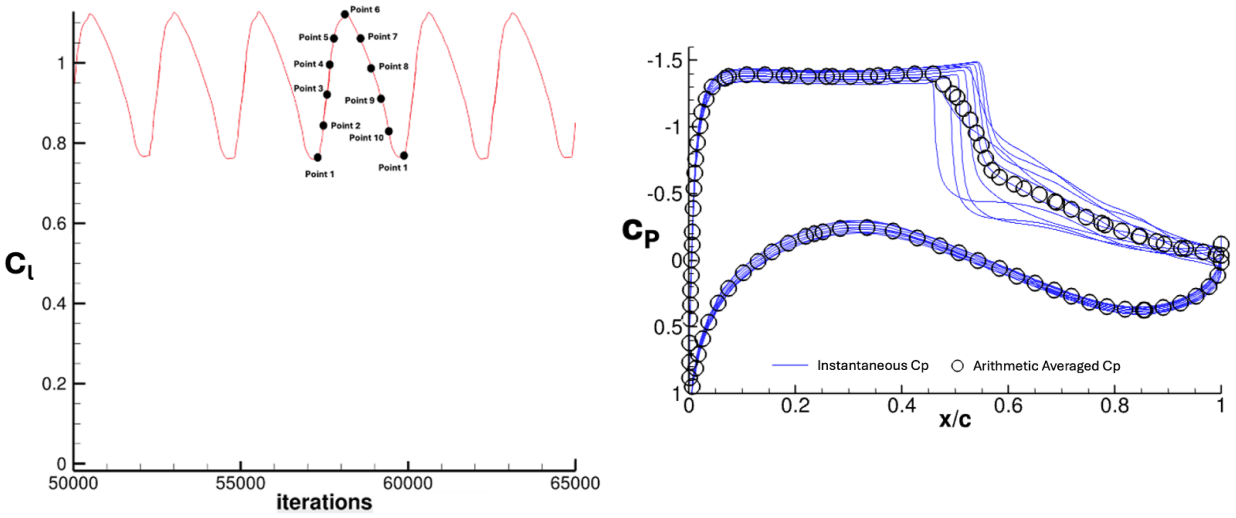

(a) Example C_l plot with the data collection points (b) Example C_p plot containing the average and individual C_p's.

Figure 13. Calculation of averaged Cp for HeldenMesh L3 solutions.

The steady C_p data from the Cadence Grids and the averaged C_p predictions from the HeldenMesh L3 grids show reasonable agreement with experiment (see Fig.14). The HeldenMesh SA-Neg predictions are slightly better than Cadence Grid SA-Neg, SA-Neg-R, and SA-Neg-QCR solutions. However, at α=2.50º for HeldenMesh L3 grid, small oscillations start to appear. All the HeldenMesh solutions exhibit low-frequency oscillations and limit cycle behavior was observed very early. Overall, both sets of grids capture the general behavior of the airfoil and are in relative agreement with experiment data prior to the onset of instabilities. Major disagreements between experiment and Cadence solutions appear as the shock front moves towards the leading edge. This behavior is captured well by the HeldenMesh grids due to their ability to resolve shock induced oscillations. URANS simulations need to be carried out by using both sets of grids to identify if buffet behavior is adequately predicted using these families of grids. Additionally, there is little to no evidence that RANS is able to accurately predict the correct physics associated with buffet even with highly resolved grids around the shock. The inability to generate a power-spectra from RANS data is also a limiting factor towards a comprehensive comparison.

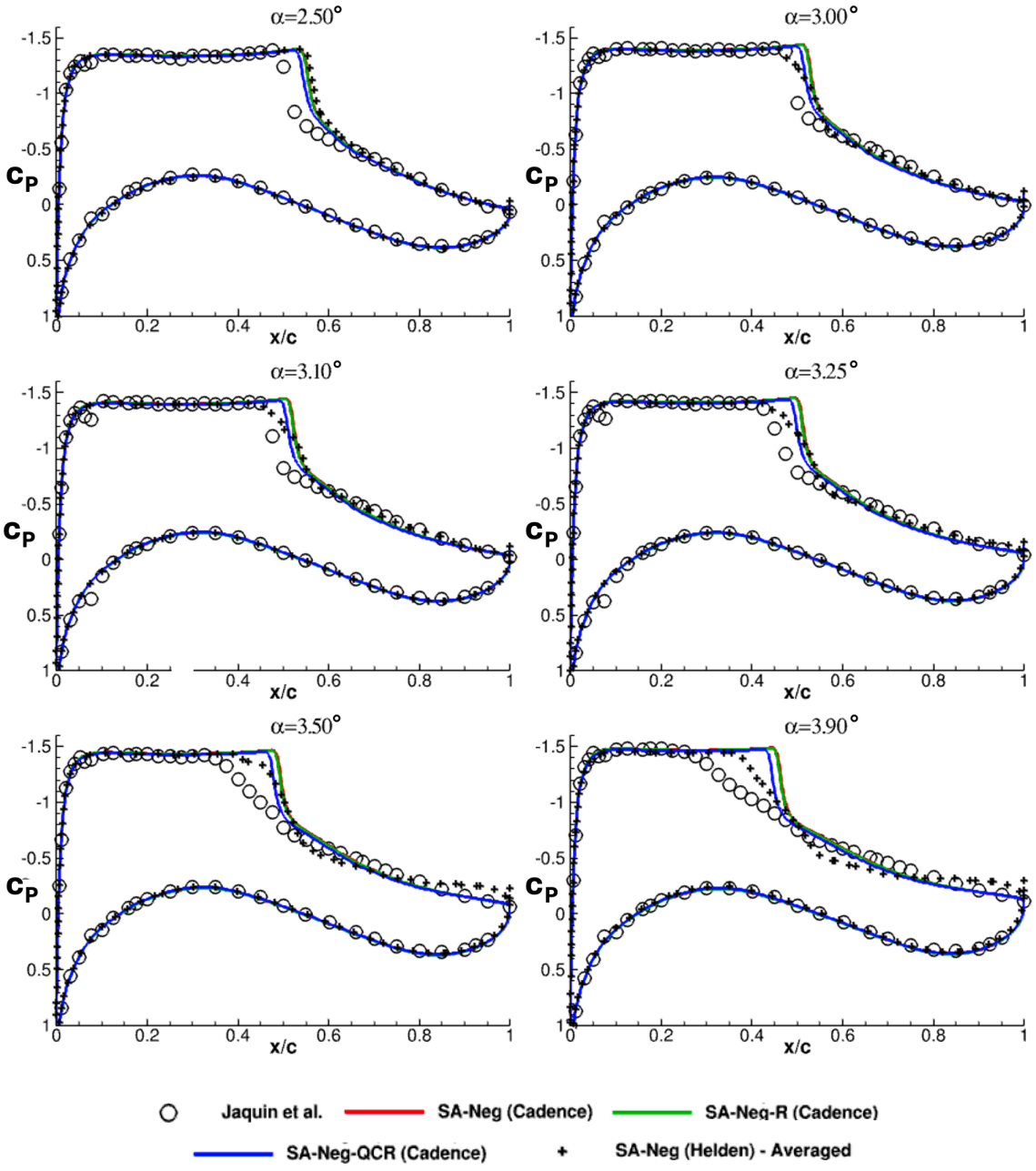

Figure 14. Cp prediction comparison between Cadence L3 and HeldenMesh L3 grids.

Figure 15 highlights the instantaneous and averaged C_p plots for the HeldenMesh L3 grid. The oscillatory motion of the shock can be observed starting at α=2.50º. Although the farthest upstream location of the shock is aft of the experimental results, results from α=2.50º suggests that RANS is able to predict instability growth that eventually leads to buffet onset. It is likely that if this time-accuracy is turned on, results would significantly improve. As α is increased, the oscillations become larger, and the shock can be observed to be as far forward as x/c=0.35 for α=3.90º. In comparison, the farthest upstream location of the shock as reported by Jacquin et al. is x/c=0.30.

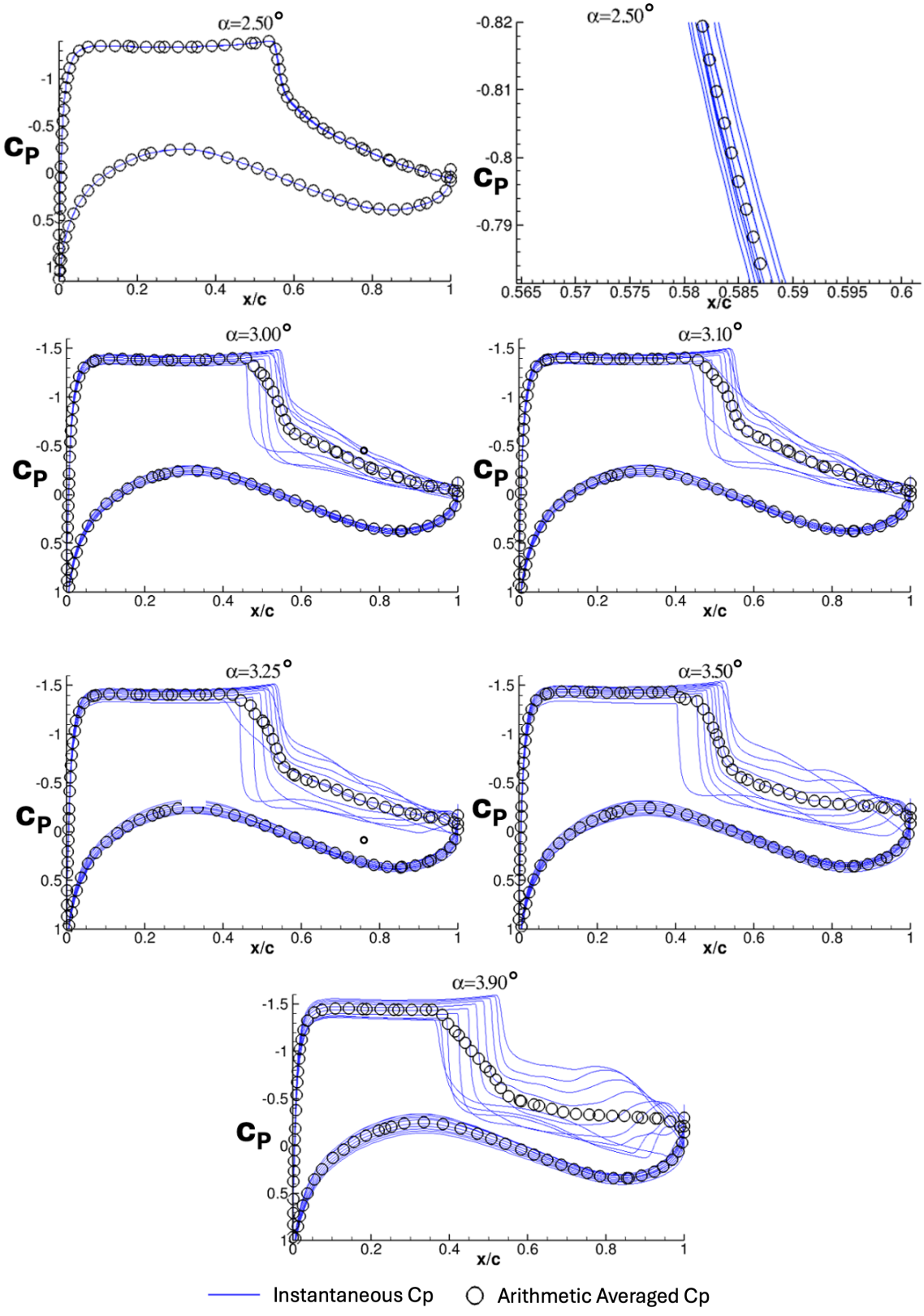

Figure 15. Cp prediction comparison for HeldenMesh L3 grid.

F. Shock Location and Shape

Contours of normalized density gradient are used to describe the shock features in Figure 16. All the shocks contain the characteristic 'lambda' foot that grows in size as the angle of attack it increased. The increase in the angle of attack also results in a larger separation zone with the shock moving towards the leading edge. Figure 16 (b) also highlights the maximum upstream and downstream locations of the shockwave relative to each other at different angles of attack.

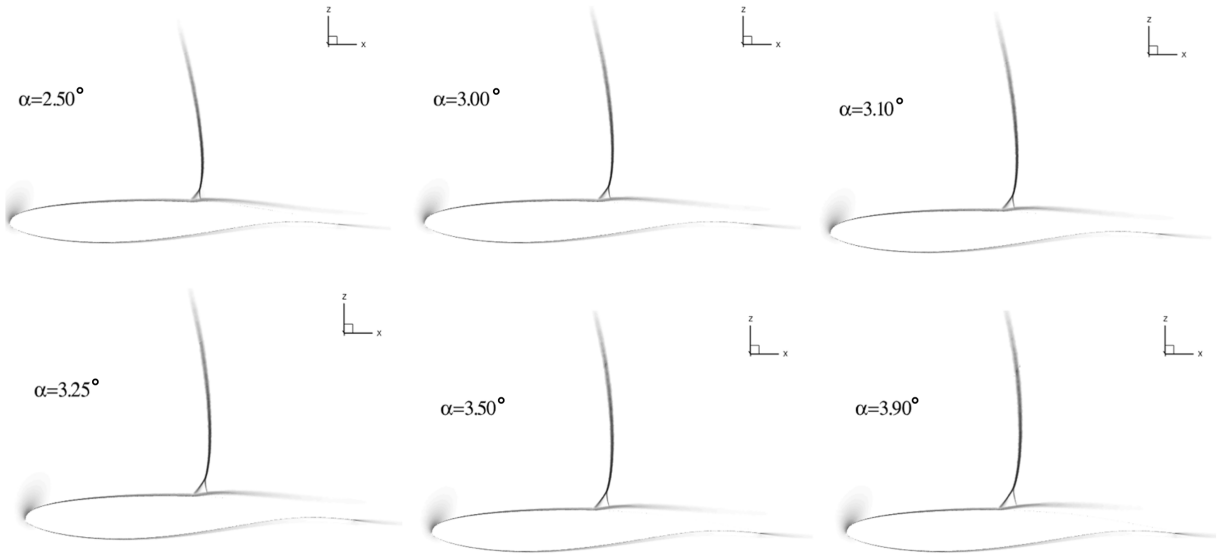

(a) Shocks at each angle of attack for Cadence L3 grid.

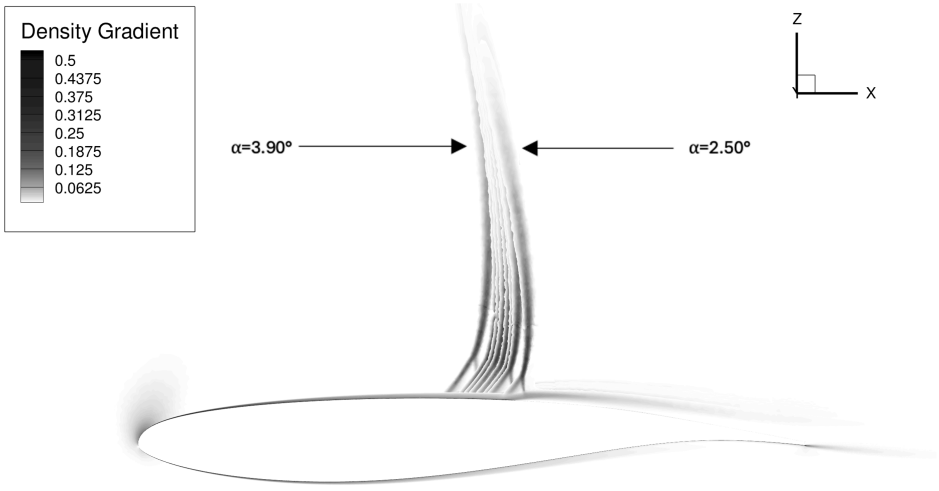

(b) Shock movement spread.

Figure 16. Shock movement from α=2.50º to α=3.90º for Cadence L3 grid.

Figure 17 shows the back-and-forth motion of the shock for the HeldenMesh grids. The location and shape are significantly different from the standing shocks that Cadence grid predicted. As the angle of attack increases, the shocks spread farther apart and larger boundary layer separation is observed. Also, the shocks predicted by the HeldenMesh grids appear to be less diffused and sharper compared to the Cadence grids.

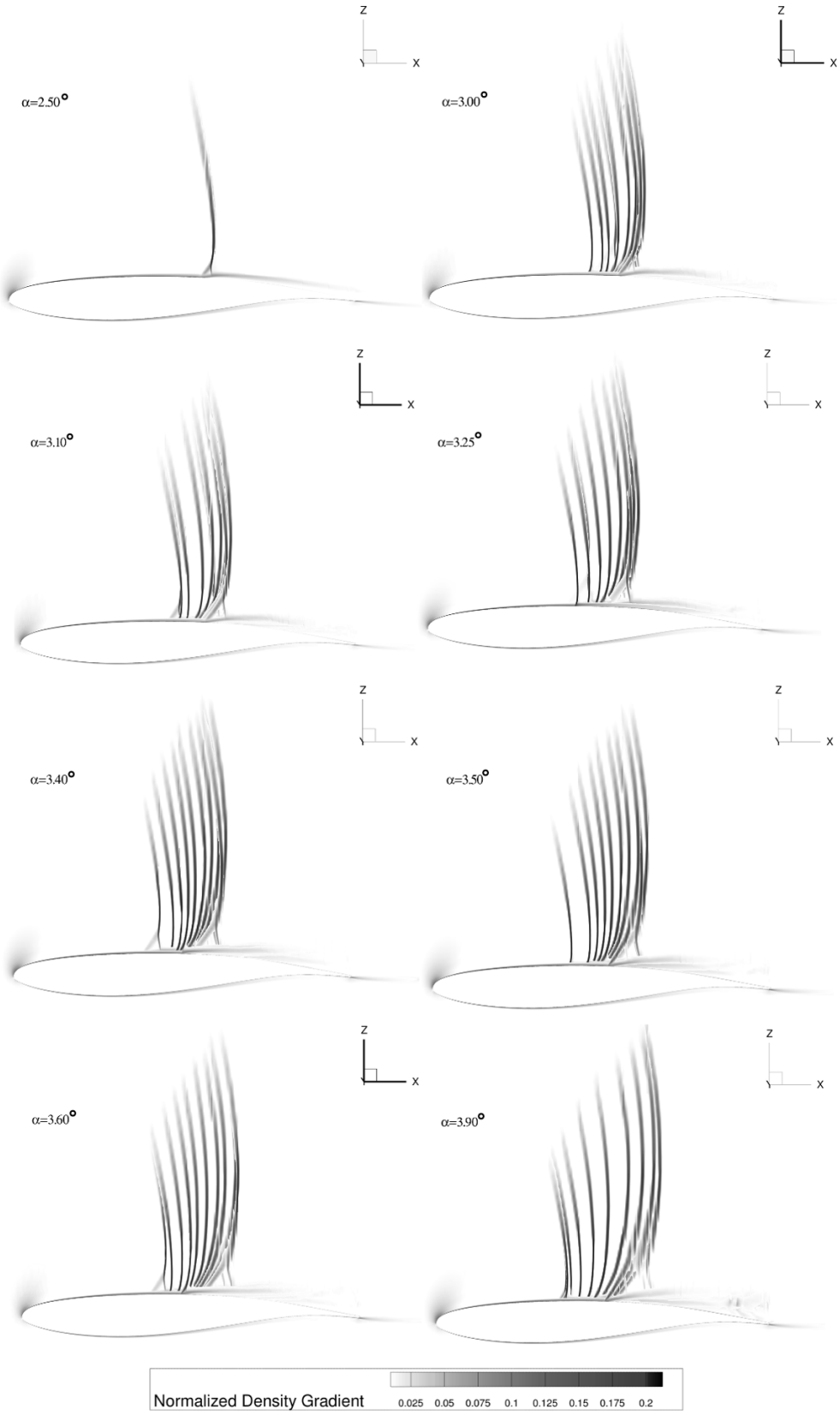

Figure 17. Shock movement for each angle of attack for HeldenMesh L3 over one oscillation cycle.

VII. Conclusions

The phenomenon of transonic buffet is an extremely challenging physical behavior that requires advanced numerical methods to capture accurately. The primary goal of this study was to investigate if RANS models are able to predict the transonic buffet with two different families of grids generated using different software and techniques. Results indicate that both the grid families predict the overall flow features with relative accuracy, however, the Cadence grid results predicted a standing shock and shows relative insensitivity to changes in grid resolution. These are typical features of a robust steady-state solution. The HeldenMesh grids on the other hand were comparatively more sensitive to changes in grid resolution primarily because the increase between successive grid levels was high in addition to the highly packed cells on the suction side of the airfoil. Despite this, grid L1 and 2 provided solutions that were comparable to their Cadence counterparts with the shock location being predict farther downstream. Grid L3 predicted large-scale unsteadiness in the flow field similar to what is expected from an unsteady solution. Convergence statistics and C_p profiles indicated that the Helden L3 solution was able to predict features associated with buffet onset which included periodic oscillations in the integrated forces and moments starting at α=2.50º, in agreement with prior experimental and numerical investigations. The buffet onset is followed by large amplitude and low frequency oscillations as angle of attack is increased. The results indicated improvements in predictive performance when compared to the Cadence solutions, however it is clear that time-accurate simulations need to be carried out for a more thorough understanding of the predictive capabilities of URANS, since much of physics is reliant on accurate time-dependent data. Overall, it is concluded that grid resolution plays an important role in predicting instabilities associated with transonic-buffet and that RANS is able to accurately predict the onset of instabilities that lead to buffet onset including some of the physical characteristics associated with buffet as long as appropriate grid, numerics, and solver combinations are utilized. However, URANS is required to be able to predict accurate physics and compare with experimental data.

VIII. Future Work

Future work using the ONERA OAT15A airfoil will include URANS study and performance comparison against numerical studies carried out in [33]. Additionally, HRL studies using time-filtering techniques [34] will be carried out since it has been shown that traditional HRL models using a static temporal filter tend to predict inaccurate stresses involving pulsatile and non-stationary flows.

References

[1] Pomeroy, B., Stanford, B, Chwalowski, P, and Rider, B, "Architecture, Scope, and Goals of the Multidisciplinary DPW-8/AePW-4 Workshop," Presentation only, AIAA Aviation 2025 Forum, 2025

[2] Brunet, V., “Computational Study of Buffet Phenomenon with Unsteady RANS Equations”, ONERA Applied Aerodynamics Department Châtillon, France

[3] Brunet, V., “Etude des instabilités aérodynamiques deprofil en transsonique à l’aide du logiciel elsa”, Internal report ONERA, April 2002.

[4] Chung, I., Lee, D., and Reu, T., “Prediction of transonic buffet onset for an airfoil with shock induced separation bubble using steady Navier Stokes solver”, 20th AIAA Applied Aerodynamics Conference, St Louis, Missouri, 24 - 26 June 2002

[5] Spalart, P.R., and Allmaras, S.R., “A one-equation turbulence model for aerodynamic flows”, La Recherche Aérospatiale, Pages 5 – 21, 1994.

[6] Menter, F.R., “Improved two-equation k-w turbulence models for aerodynamic flows”, Technical report, NASA Technical Memorandum 103975, October 1992.

[7] Shih, T., Zhu, J., and Lumley, L., “A realisable Reynolds stress algebraic equation model”, TM105993 ICOMP92-27, CMOTT92-14. NASA 1992

[8] Deck, S., “Numerical simulation of transonic buffet over a supercritical airfoil”, *AIAA journal*, *43*(7), 1556-1566, 2005

[9] Walters, D.K., Bhushan, S., Alam, M.F. et al. Investigation of a Dynamic Hybrid RANS/LES Modelling Methodology for Finite-Volume CFD Simulations. Flow Turbulence Combust 91, 643–667 (2013). https://doi.org/10.1007/s10494-013-9481-9

[10] Jamal, T, Shobayo, OO, and Walters, DK. "A New Variant of the Dynamic Hybrid RANS-LES Model for Complex Turbulent Flows." Proceedings of the ASME 2021 International Mechanical Engineering Congress and Exposition. Volume 10: Fluids Engineering. Virtual, Online. November 1–5, 2021. V010T10A052.

ASME. https://doi.org/10.1115/IMECE2021-72185
[11] Jamal, T, & Walters, DK. "A Dynamic Time Filtering Technique for Hybrid RANS-LES Simulation of Non-Stationary Turbulent Flow." Proceedings of the ASME-JSME-KSME 2019 8th Joint Fluids Engineering Conference. Volume 2: Computational Fluid Dynamics. San Francisco, California, USA. July 28–August 1, 2019. V002T02A051. ASME. https://doi.org/10.1115/AJKFluids2019-4696
[12] Jamal, T., Shobayo, O., Walters, D. K., and Bhushan, S. (March 14, 2025). "Static and Dynamic Time Filtering Techniques for Hybrid RANS-Large Eddy Simulation of Non-Stationary Turbulent Flows." ASME. J. Fluids Eng. August 2025; 147(8): 081502. https://doi.org/10.1115/1.4067790
[13] Hass, R., Housman, J.A., Stich, G., Sozer, E., and Duensing, J., "Wall-Modeled Large Eddy Simulations of Transonic Buffet Over a Supercritical Airfoil," AIAA 2024-4263. AIAA AVIATION FORUM AND ASCEND 2024 . July 2024.
[14] Browne, O.M., Maldonado, D., Housman, J.A., Duensing, J., and Milholen, W.E., "Simulating Transonic Buffet Aerodynamics for the Boeing Transonic Truss-Braced Wing Aircraft," AIAA 2024-0065. AIAA SCITECH 2024 Forum. January 2024.
[15] Maldonado, D., Housman, J.A., Dumlupinar, E., Stich, G., Duensing, J., and Milholen, W.E., "Evaluation of a Physics-Based Unsteady RANS Method for Buffet Onset Prediction," AIAA 2024-3639. AIAA AVIATION FORUM AND ASCEND 2024, July 2024.
[16] Penner, C.D., Housman, J. A., Stich, G., Koch, J. R., and Duensing, J., "Wall-Modeled Large-Eddy Simulations of a Swept Wing," AIAA SCITECH 2024 Forum, 2024, p. 2376.
[17] Ducros, F., Ferrand, V., Nicoud, F., Weber, C., Darracq, D., Gacherieu, C., and Poinsot, T., "Large-eddy simulation of the shock/turbulence interaction," Journal of Computational Physics, Vol. 152, No. 2, 1999, pp. 517–549.
[18] Spalart, P., Shur, M., Strelets, M., and Travin, A., "Sensitivity of landing-gear noise predictions by large-eddy simulation to numerics and resolution," 50th AIAA aerospace sciences meeting including the new horizons forum and aerospace exposition, 2012, p. 1174.
[19] Mary, I., and Sagaut, P., "Large eddy simulation of flow around a high lift airfoil," Direct and Large-Eddy Simulation IV, 2001, pp. 157–164.
[20] Wick, A., and Hooker, R., "HeldenMeshUsersManualVersion3.05", Helden Aerospace Corporation, June 2018.
[21] Pita, C. "DPW-8: ONERA OAT15A Meshes (Test Case 1): Fidelity Pointwise." July 16, 2024.
[22] Jacquin, L., Molton, P., Deck, S., Maury, B., and Soulevant, D., "Experimental Study of Shock Oscillation over a Transonic Supercritical Profile," AIAA Journal, Vol. 47, No. 9, 2009, pp. 1985–1994. https://doi.org/10.2514/1.30190.
[23] Jamal, T., Kelly, S., Hunter, C., Milholen, W., Wignall, T.J., Krist, S., "Simulation of the Transonic Truss-Braced Wing High-Lift Configuration at Mach 0.2 using USM3D-Mixed Element Solver," AIAA Aviation 2025 Forum, 2025
[24] Allmaras, S. R., Johnson, F. T., and Spalart, P. R., "Modifications and Clarifications for the Implementation of the Spalart-Allmaras Turbulence Model," ICCFD7-1902, 7th International Conference on Computational Fluid Dynamics, Big Island, Hawaii, 9-13 July 2012
[25] Dacles-Mariani, J., Kwak. D., and Zilliac, G., "On numerical errors and turbulence modeling in tip vortex flow prediction," International journal for numerical methods in fluids 30.1 (1999): 65-82.
[26] Dacles-Mariani, Jennifer, et al. "Numerical/experimental study of a wingtip vortex in the near field." AIAA journal 33.9 (1995): 1561-1568.
[27] Spalart, P. R., "Strategies for Turbulence Modelling and Simulation," International Journal of Heat and Fluid Flow, Vol. 21, 2000, pp. 252–263.
[28] Pandya, M. J., Frink, N. T., Ding, E., and Parlette, E. B., "Toward Verification of USM3D Extensions for Mixed Element Grids," AIAA Paper 2013-2541, 31st Applied Aerodynamics Conference, San Diego, CA, June 2013; DOI: 10.2514/6.2013-2541
[29] Pandya, M. J., Diskin B., Thomas, J. L., and Frink N. T., "Improved Convergence and Robustness of USM3D Solutions on Mixed Element Grids," AIAA Journal (2016), 54(9), pp. 2589-2610; DOI: 10.2514/1.J054545
[30] Pandya, M. J., Diskin B., Thomas, J. L., and Frink N. T., "Assessment of USM3D Hierarchical Adaptive Nonlinear Method Preconditioners for Three-Dimensional Cases," AIAA Journal (2017) 55(10), pp. 3409-3424; DOI:10.2514/1.J055823
[31] Pandya, M. J., Jespersen, D. C., Diskin B., Thomas, J. L., and Frink, N. T., "Efficiency of Mixed-Element USM3D for Benchmark Three-Dimensional Flows," AIAA Journal (2021), 59(8), pp. 2997-3011; DOI: 10.2514/1.J059720
[32] Pandya, M. J., Jespersen, D. C., Diskin B., Thomas, J. L., and Frink, N. T., "Verification and Scalability of Mixed-

Element USM3D for Benchmark Three-Dimensional Flows," AIAA Journal (2021), 59(11), pp. 4719-4738; DOI: 10.2514/1.J060064

[33] Steve Lamberson, Brent Pomeroy, and Tausif Jamal. "Simulations for the DPW-8/AePW-4 Static Aeroelastic Deformation and Buffet Working Groups: Part 1." Scheduled for presented at AVIATION 2025. July 23, 2025.

[34] Jamal, T., Shobayo, O., Walters, D. K., and Bhushan, S. (March 14, 2025). "Static and Dynamic Time Filtering Techniques for Hybrid RANS-Large Eddy Simulation of Non-Stationary Turbulent Flows." ASME. *J. Fluids Eng*. August 2025; 147(8): 081502. https://doi.org/10.1115/1.4067790